Research Square

Preprints are preliminary reports that have not undergone peer review.
They should not be considered conclusive, used to inform clinical practice,
or referenced by the media as validated information.

Frequency-Dependent Electrical Behavior of Al/CuO/n-Si Schottky Barrier Diodes: Interface-State Analysis and Series-Resistance Effects

İdris Candan

idris.candan@kocaeli.edu.tr

Kocaeli University

Fatih Mehmet Coşkun

Istanbul Medeniyet University

Sabreen A. HAMEED

Gazi University

AL-EDRESİ Abeer

Kocaeli University

Sait Eren San

Kocaeli University

Şemsettin Altındal

Gazi University

Research Article

Keywords: Schottky photodiode, CuO interlayer, frequency-dependent electrical characterization, interface trap density (Nit), low-high frequency capacitance (CLF-CHF) model, and dielectric relaxation

Posted Date: November 20th, 2026

DOI: https://doi.org/10.21203/rs.3.rs-11658301/v1

License: This work is licensed under a Creative Commons Attribution 4.0 International License.
Read Full License

Additional Declarations: No competing interests reported.

Frequency-Dependent Electrical Behavior of Al/CuO/n-Si Schottky Barrier Diodes: Interface-State Analysis and Series-Resistance Effects

[1]İdris CANDAN ,[2]Fatih Mehmet COŞKUN, [3,4]Sabreen A. HAMEED, [1,5]Abeer AL-EDRESİ, [1]Sait Eren SAN, [3]Şemsettin ALTINDAL

[1]Department of Physics, Faculty of Arts and Sciences, Kocaeli University, 41001, Kocaeli, Türkiye
[2] Department of Physics Engineering, Istanbul Medeniyet University, Istanbul, 34700, Türkiye
[3]Department of Physics, Faculty of Science, Gazi University, Ankara, Türkiye
[4]Department of Physics, College of Science, University of Diyala, Diyala, Iraq
[5]Department of Physics, Faculty of Sciences, Hodeidah University, Hodeidah, Yemen

Abstract

In this work, an Al/CuO/n-Si/Ag heterostructure was fabricated using physical vapor deposition and radio-frequency sputtering. Its voltage- and frequency-dependent electrical properties were systematically investigated from capacitance–voltage (*C-V*) and conductance–voltage (*G/ω-V*) measurements performed over a wide range of frequencies and applied voltages. The electronic parameters were also analyzed at different frequencies to investigate how they change with frequency. The interface trap density *(Nit*) values were obtained using the low-high frequency capacitance (C_{LF}-C_{HF}) model, the Hill–Coleman method, and the parallel conduction method. The results showed a strong dependence of capacitance and conductance on both applied voltage and frequency, particularly at low and intermediate frequencies. The observed dispersion is mainly related to the response of the interface states and dielectric relaxation, while the effect of the series resistance becomes more evident at higher frequencies and in the accumulation region. The barrier height (Φ_B), depletion width (W_D), and electric field (E_m) obtained from the measurements showed a clear dependence on frequency. Since the effect of series resistance becomes more significant at high frequencies, the 1 MHz data were corrected for the series resistance before further analysis. The analysis shows that *Nit* has a stronger effect on the device response in the depletion and inversion regions at low frequencies. At high frequencies, the effect of series resistance plays a dominant role, particularly in the accumulation region. The values of *Nit* obtained from the three methods were not the same, showing that the calculated interface-state density can vary depending on the model and measurement conditions. Therefore, both interface states and series resistance need to be considered when analyzing the electrical characteristics of CuO/n-Si-based Schottky diode structures.

Keywords: Schottky photodiode, *CuO* interlayer, frequency-dependent electrical characterization, interface trap density (*Nit*), low-high frequency capacitance (C_{LF}-C_{HF}) model, and dielectric relaxation.

***Correspondence should be addressed to**: idris.candan@kocaeli.edu.tr

Highlights:

- High-quality Al/CuO/n-Si Schottky barrier diode were successfully fabricated using *RF* sputtering and *PVD* techniques.
- Frequency-dependent electrical behavior was governed by the combined effects of interface traps and series resistance.
- Interface trap density was accurately quantified using three independent methods, demonstrating excellent agreement.
- Correction of series resistance effects significantly improved the accuracy of capacitance and conductance analyses.

1. Introduction

Copper oxide (CuO) thin films and nanostructures have been widely studied over recent decades due to their versatile physical properties and potential applications in optoelectronic devices, energy conversion systems, gas sensors, and catalysis [1-7]. The interest in metal oxide semiconductors is largely related to their low cost, earth abundance, environmental compatibility, and tunable electrical and optical properties [8-11]. CuO is a p-type semiconducting with a band gap has been reported in the range of approximately 1.1 - 2.1 *eV*, depending on the preparation conditions and structural properties, and has been investigated for various applications, including gas sensors, solar cells, photoelectrochemical devices, and energy storage systems [12,13] [14-17] [18-25]

The electrical and optoelectronic properties of CuO-based devices are strongly influenced by the fabrication conditions, which can modify the defect density, band structure, and carrier transport properties [23,24]. CuO-based heterostructures, particularly CuO/Si, structures, have also been investigated due to their favorable charge-transport and optoelectronic properties [26-31].

However, the electrical behavior of these devices is strongly influenced by film stoichiometry, interface quality, and defect formation during growth processes [6].

A major factor limiting the electrical performance of CuO-based devices is the presence of interface-related effects, particularly in metal–semiconductor (*MS*) and metal–interlayer–semiconductor (*MIS*) Schottky structures. The performance of these structures is strongly affected by the interfacial layer, such as barrier height, interface state density, series resistance, and ideality factor [32, 33]. In thin film transistor applications, CuO has also attracted attention as a p-type channel material, while p-type oxide TFTs generally suffer from low mobility and poor switching characteristics [1-5] [6,7].

Recent studies have also shown that the electrical and photovoltaic properties of CuO/n-Si-based Schottky structures are strongly influenced by material parameters such as CuO thickness, bandgap, electron affinity, carrier concentration, and defect density [34]. More recently, Jagadish et al. investigated Cu_2O/TiO_2 heterojunctions using *C-V*, *C-f*, and impedance spectroscopy techniques to understand the effect of interfacial defects on charge transport mechanisms and frequency-dependent electrical behaviour [35] Their results showed that the interface defects strongly affected frequency dispersion, charge accumulation, and polarization, highlighting the importance of frequency-dependent electrical characterization of understanding charge transport in copper oxide-based junctions [35].

In this work, the electrical behavior of Al/CuO/n-Si Schottky diodes was investigated as a function of applied voltage and frequency at room temperature. Particular attention is given to the interface state density (*Nit*), series resistance (*Rs*), and surface charge effects, as well as their dependence on the applied voltage and frequency. The electrical characterization was performed using *C–V* and G/ω–*V* measurements over a wide frequency range (0.1 *kHz*–1 *MHz*). The low- and high-frequency capacitance (C_{LF}-C_{HF}) model, the Hill–Coleman method, and the parallel conduction method were employed to determine the interface-state density and evaluate the series resistance in metal–semiconductor systems [36]. The main focus of this study is to examine the relationship between interface-state density, surface-charge effects, and series resistance using frequency-dependent *C-V* and G/ω-*V* measurements. Using three different approaches to determine *Nit* also allows the consistency of the extracted interface-state parameters to be assessed and their differences to be compared. The obtained results help clarify the frequency-dependent electrical

behavior of the CuO/n-Si-based Schottky diode structure and highlight the influence of interface-related effects.

2. Experimental Details

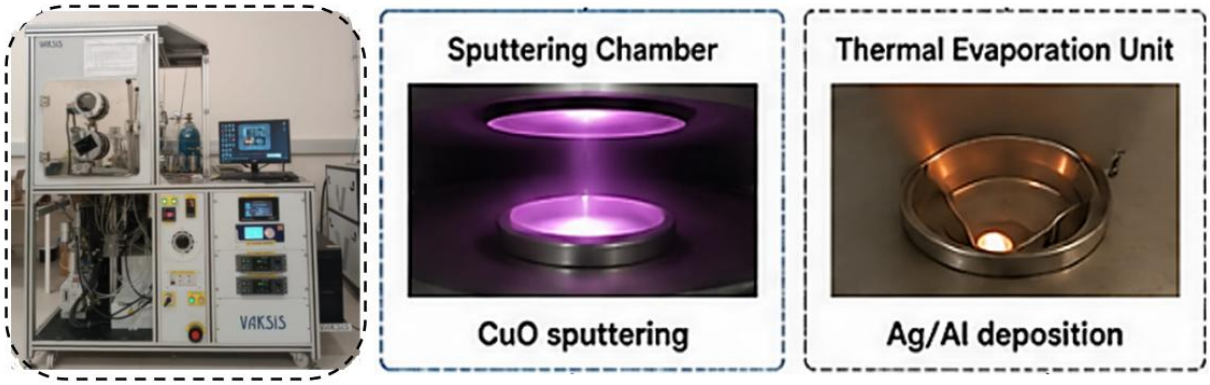
The Al/CuO/n-Si Schottky barrier diode (SBD*)* was fabricated using thermal evaporation and the *RF* magnetron sputtering technique. Phosphorus-doped (*P*-doped) n-type *Si* (100) wafers with a resistivity of 3.5-5.4 *Ω*.cm were used as semiconductor substrates. Before deposition, the *Si* substrates were chemically cleaned to remove organic contaminants and surface impurities. The cleaning solution was prepared by mixing 325 mL of distilled water with 65 mL of ammonium hydroxide (NH_4OH), and the mixture was heated to 70 °C. After the solution was removed from the hot plate, 65 mL of hydrogen peroxide (H_2O_2) was added. The substrates were subsequently immersed in the prepared solution for 15 min and rinsed several times with distilled water. The substrates were subsequently immersed in warm acetone for 10 min and then in methanol for 5 min. Finally, the they were rinsed with deionized water and dried under nitrogen flow.

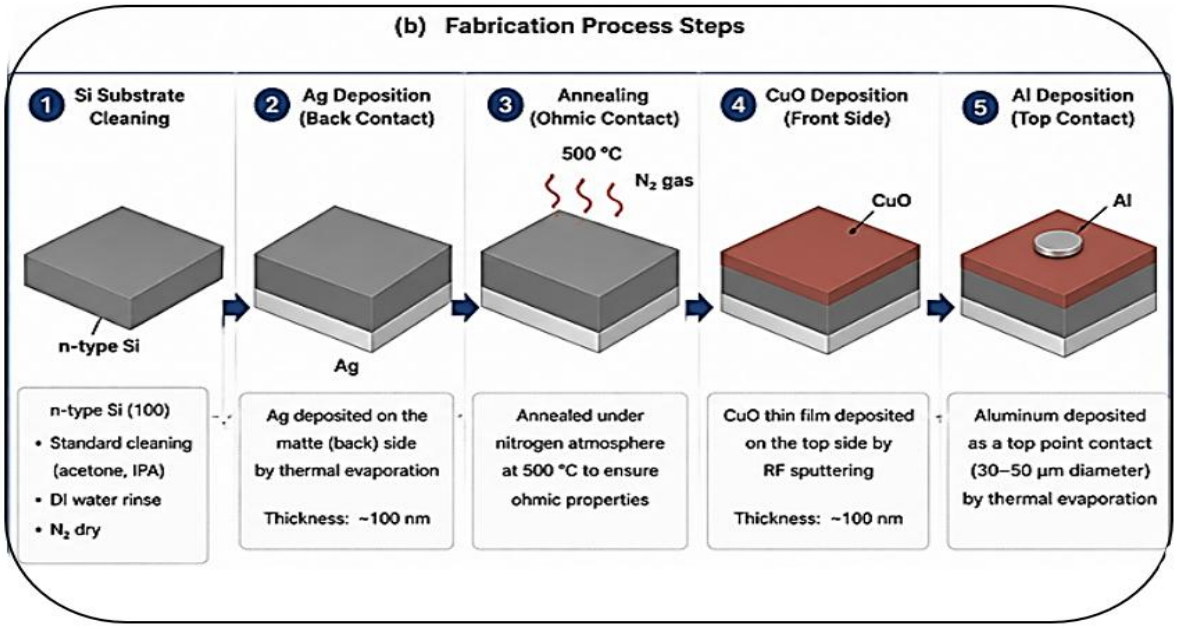
The deposition process was carried out using the VAKSIS multifunctional *PVD* system. A high-purity Ag (99.99%) layer was deposited on the non-polished of the Si substrate by thermal evaporation and subsequently annealed at 500°C under a nitrogen atmosphere to obtain the stable ohmic contact. A CuO thin film with thickness of approximately 100 *nm* was then deposited on the polished side of the Si substrate by RF magnetron sputtering. The deposition was performed at an RF power of 200 W using Ar gas at a flow rate of 25 cm^3/min. The working pressure was maintained in the range of 26.2 - 30.2 mTorr, with a target-to-substrate distance of 20 cm. During deposition, the substrate holder was rotated at 5 rpm.

Finally, Al top contacts with a thickness of 30-50 *nm* were deposited by thermal evaporation through a shadow mask, completing the Ag/n-Si/CuO/Al Schottky diode structure. The diameter of circular Al contact was 0.21 cm, and this value used in the C-V and interface state calculations.

The fabricated Al/CuO/n-Si SBDs were electrically characterized at room temperature using frequency-dependent *C-V* and *G/ω-V* measurements over a wide frequency range of 0.1 kHz to 1MHz. The barrier height (Φ_B), donor concentration (N_d), series resistance (R_s), interface-state density (*Nit*), depletion width (W_D), and maximum electric field (E_m), were extracted from the

measured data. Figure 1 illustrates the fabrication system, fabrication sequence, and final device structure, while Figure 2 shows the schematic energy-band diagram of the fabricated Al/CuO/n-Si SBD.





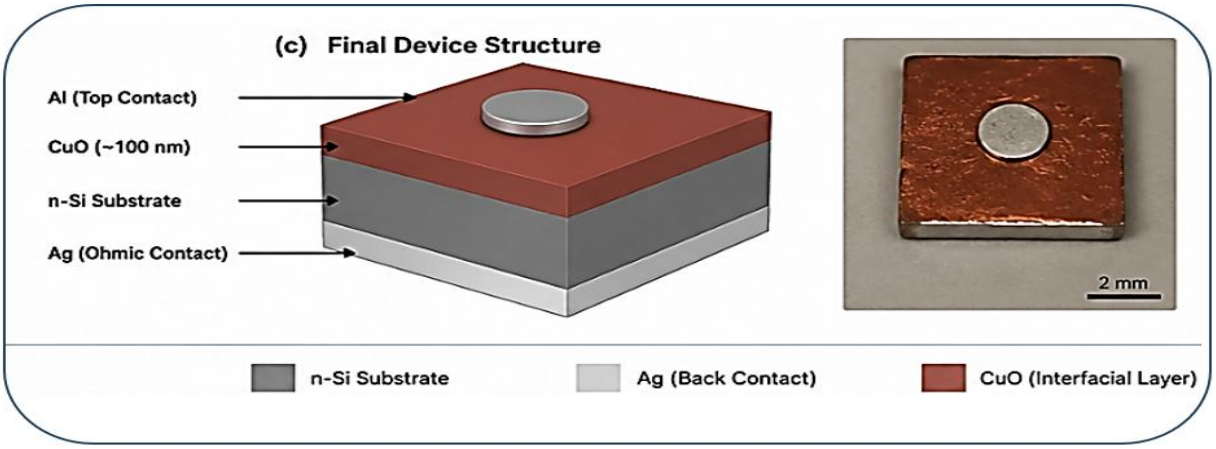


Figure 1. Fabrication of the Al/CuO/n-Si *SBD*: **(a)** PVD system used for deposition, **(b)** schematic illustration of the fabrication steps, and **(c)** schematic and photograph of the final device structure.

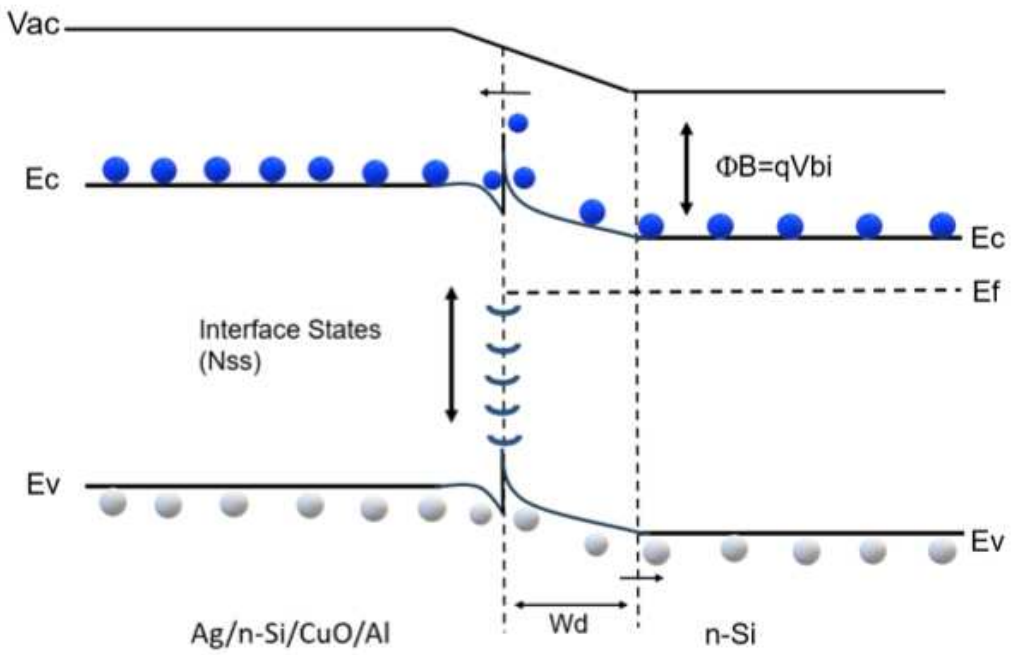


Figure 2. Schematic energy-band diagram of fabricated Al/CuO/n-Si *SBD* structure, showing the depletion region and interface states.

3. Results and Discussion

3.1. Structural Characterization

Cross-sectional SEM and Compositional Analysis

Figure 3 shows cross-sectional SEM images of the CuO film deposited on a Si wafer at different magnifications. In Fig. 3(a), the Si substrate can be seen across the imaged region, while the CuO coating is visible along its upper surface. The interface between the film and the substrate becomes clearer at higher magnifications. As seen in Fig. 3(b), the interface is not completely flat and shows some local variations, which may be partly due to the roughness of the Si wafer images in Figs. 3(c) and 3(d) provide a closer look at the film morphology and the interface with the Si substrate. The upper surface of the film appears relatively rough, and the interface shows local irregularities. These features suggest that the film/substrate boundary is not perfectly uniform. However, the contrast variations observed in the SEM images alone are not sufficient to determine whether they result from interdiffusion, the formation of an intermediate layer, or local compositional differences. In general, the SEM images provide useful information about the cross-sectional morphology of the CuO/Si structure. Although the film and substrate can be distinguished in the images, further compositional and structural analyses are needed to confirm the nature of the deposited layer and to better understand the interface.

The elemental composition of the prepared samples was investigated using energy-dispersive X-ray spectroscopy (EDS). To evaluate the relative contributions of copper (Cu) and oxygen (O), the detected elemental concentrations were renormalized to exclude signals attributed to the substrate and other non-target elements. The resulting values are presented in Table 1.

As shown in Table 1, the renormalized mass concentrations of Cu and O are 57.47 wt.% and 42.53 wt.%, respectively. The corresponding atomic concentrations yield an O/Cu ratio of approximately 2.94, which is considerably higher than the theoretical ratio of 1 expected for stoichiometric CuO. This difference indicates that the measured elemental composition does not directly correspond to the theoretical stoichiometry of pure CuO. Although this deviation may be related to limitations of quantitative EDS analysis and measurement conditions, the available data are insufficient to determine its precise origin. Therefore, the EDS results confirm the presence of Cu and O in the

analyzed region but are not sufficient on their own to establish the formation or stoichiometry of the CuO phase.

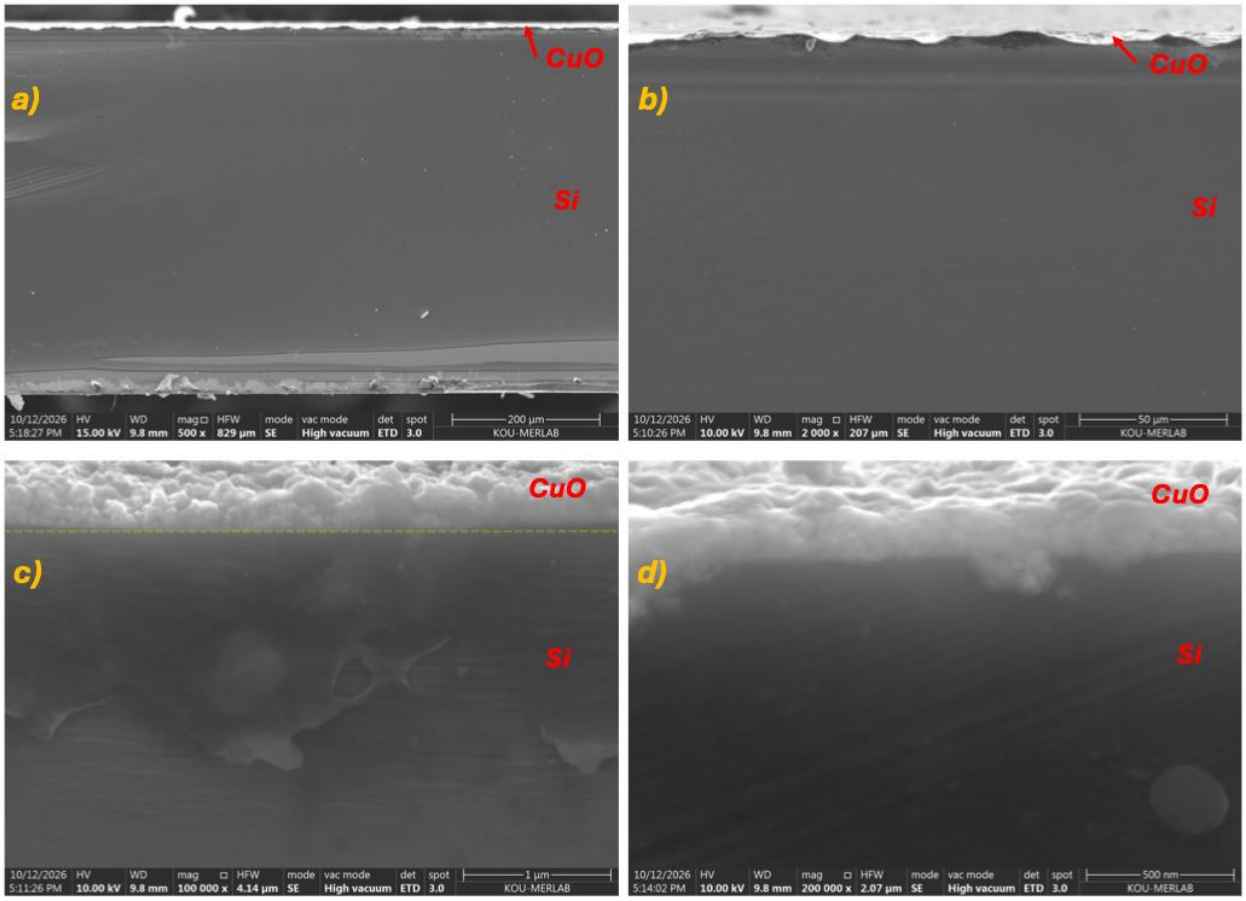


Figure 3. Cross-sectional scanning electron microscopy (SEM) images of the CuO thin film deposited on a Si wafer at different magnifications: (a) overview of the cross section at 500x, (b) enlarged cross-sectional view at 2000x, (c) interface morphology at 100000x, and (d) higher-magnification view of the coating/substrate interface at 200000x. *The dashed line in panel (c) indicates the approximate position of the interface between the CuO thin film and the Si substrate.*

Table 1. EDS-derived elemental composition of Cu and O, renormalized to 100%.

Element	***Renormalized Mass Concentration (wt.%)***	***Renormalized Atomic Concentration (at.%)***
Cu	57.47	25.38
O	42.53	74.62
Total	100.00	100.00

3.2.Electrical Characterization

The electrical characteristics of the fabricated Al/CuO/n-Si structure were investigated using frequency-dependent *C-V* and *G/ω-V* measurements. The measured capacitance-voltage characteristic can be divided into three regions over the investigated bias range: inversion (-2 to -0.5 *V*), depletion (-0.5 to 1.9*V*), and accumulation (1.9 to 3*V*) as given in Fig. 4 (a, b). As shown in Fig. 4 (a), the capacitance remains low and changes only slightly with bias voltage in the region assigned to inversion. This behavior may be associated with an increase in the effective width, which reduces the measured capacitance according to ($C = \varepsilon A/\omega$).

In the depletion region, the capacitance increases with applied voltage, which may be related to changes in the depletion witdth and contribution of the interface states. At low frequency, a distinct capacitance peak of approximately $2.2\text{x}10^{-7}$ *F* appears around 1.6-1.8 *V.* This peak suggests a contribution electrically active interface states or trapped charges, although other effects, including interfacial polarization and series resistance, may also influence the measured response. At low frequencies, interface states can respond more effectively to the AC signal and contribute to the measured capacitance through charge exchange with the semiconductor. As the frequency increases from 0.1 *kHz* to 7 *kHz*, a peak becomes less pronounced. This behavior is consistent with a reduced contribution from interface states that cannot be respond fully to the faster AC signal. A slight shift in the peak position is also observed with frequency. This shift may be related to charge redistribution, relaxation processes, and the influence of series resistance. In the accumulation region, the capacitance decreases under some measurement conditions. This behavior may reflect the combined effects of interface states, polarization, and series resistance. However, the contribution of each mechanism cannot be determined from the C-V curves alone.

At the high frequencies, the capacitance remains relatively low over the depletion region and then increases with applied voltage, reaching a miximum. At higher bias voltages, the capacitance decreases gradually, and differences between the frequency-dependent curves become apparent. These variations may be associated with the combined effects of interface states, polarization, and series resistance. In the accumulation region, the capacitance becomes relatively stable at higher frequencies, suggesting a reduced contribution from processes that cannot follow the AC signal. The *G/ω-V* characteristics also vary with applied voltage and frequency, indicating that the measured conductance response is frequency-dependent. The frequency-dependent response may

be partly associated with electrically active interface states, which can contribute additional capacitance and conductance at low frequency. The effects of series resistance and interfacial layer should also be considered.

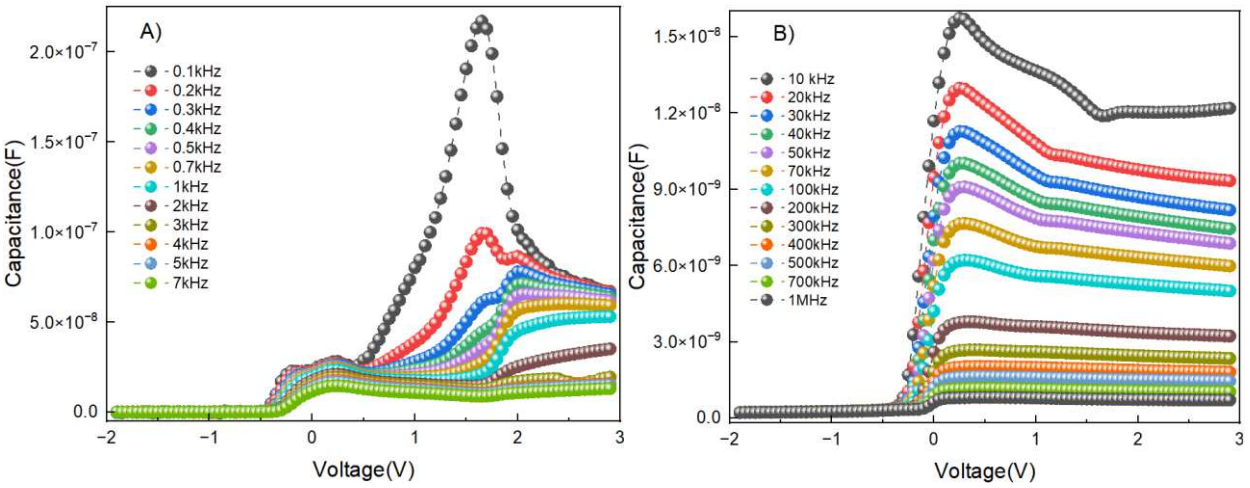


Figure 4. The *C-V* characteristics of the Al/CuO/n-Si *SBD* at **(a)** lower frequencies (0.1–7 *kHz*) and **(b)** higher frequencies (10-1000 *kHz*).

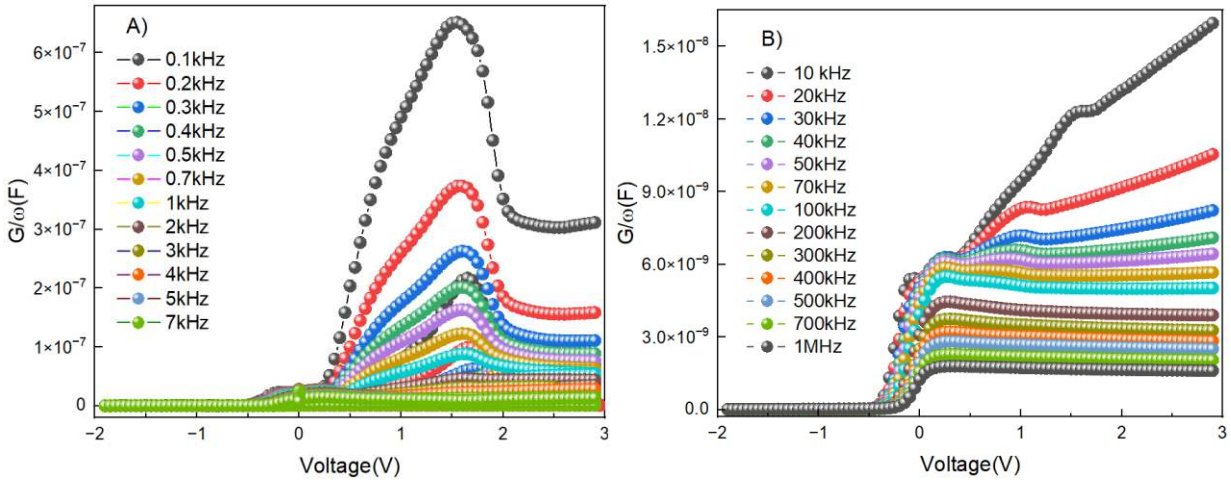


Figure 5. The G/ω–V characteristics of the Al/CuO/n-Si *SBD* at **(a)** lower frequencies (0.1–0.7 kHz) and **(b)** higher frequencies (10–30 kHz).

To investigate the frequency dependance of electrical parameters, including N_D, E_F, V_D, Φ_B, W_D, and Em, the C^{-2} characteristics as a function of V were analyzed under reverse-bias conditions over

the frequency range of 20 *kHz* to 1 *MHz*, as shown in Figure 6. Under the depletion approximation, the relationship between C-2 and applied reverse-bias voltage can be expressed as follows:

$$\frac{1}{C^2} = \frac{2}{q\varepsilon_s\varepsilon_o A^2 N_D} V_R \tag{1}$$

Here, (A) is the area of the rectifying contact, ε_s is the relative permittivity of the semiconductor, ε_0 is the vacuum permittivity, and V_R is the applied reverse-bias voltage.

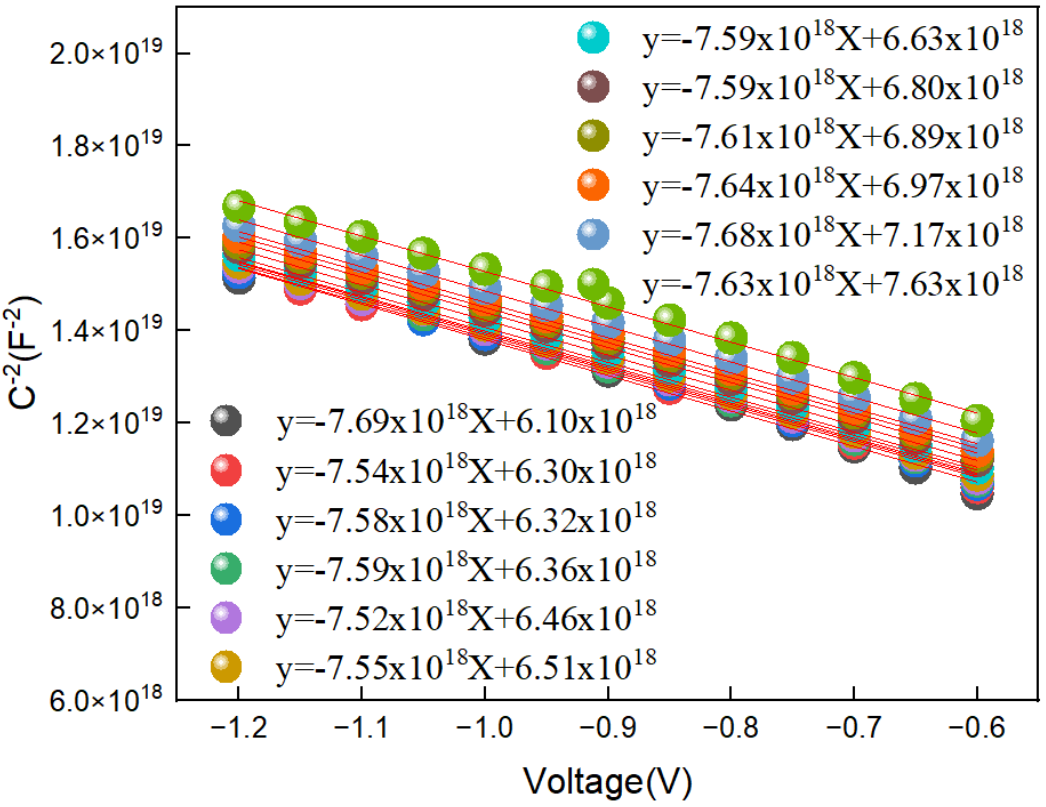


Figure 6. The C^{-2}- V plots of the Al/CuO/n-Si *SBD* structure at various frequencies.

The slope of the linear region of the C^{-2}-V plots was used to determine the donor concentration, N_D, according to following expression:

$$\tan(\theta) = \frac{d(C^{-2})}{dV} = \frac{2}{qA^2\varepsilon_s\varepsilon_o N_D} \tag{2}$$

The donor concentration, N_D, was calculated at each investigated frequency using Eq. (2). Using the calculated N_D and the effective density of states in the conduction band ($N_C = 2.8 \times 10^{19}$ cm^{-3}

for *Si* at room temperature), the Fermi-level position was estimated using the following equation (Eq. (3)) [4]:

$$E_F = (\frac{kT}{q}).ln\left(\frac{N_c}{N_d}\right) \quad (3)$$

The intercept voltage, (Vo), obtained by extrapolating the linear region of the C^{-2}-V plot to (C^{-2} =0), was used to calculate the diffusion potential according to (V_D = Vo + kT/q). The values of Φ_B, W_D, and E_m were calculated using the extracted *Vo* and V_D values. The results are summarized in Table 2.

$$\Phi_B(CV) = (V_o + \frac{kT}{q}) + E_F = V_D + E_F \quad (4a)$$

$$W_d = \left(\frac{2\varepsilon_s\varepsilon_o V_d}{qN_d}\right)^{1/2} \quad (4b)$$

$$E_m = (\frac{2qN_dV_o}{\varepsilon_s\varepsilon_o})^{1/2} \quad (4c)$$

Table 2. Summary of the main electrical parameters extracted from the reverse-bias C^{-2}-V characteristics at various frequencies.

Frequency (kHz)	***V_0(V)***	***N_d(cm^3)***	***E_F(eV)***	***ΦB(eV)***	***W_D(cm)***	***E_m(V/cm)***	***V_D(eV)***
20	$7.92x10^{-1}$	$1.58x10^{15}$	$2.45x10^{-1}$	1.06	$8.10x10^{-5}$	$2.13x10^{4}$	0.817
30	$8.36x10^{-1}$	$1.61x10^{15}$	$2.44x10^{-1}$	1.10	$8.24x10^{-5}$	$2.21x10^{4}$	0.861
40	$8.35x10^{-1}$	$1.60x10^{15}$	$2.44x10^{-1}$	1.10	$8.25x10^{-5}$	$2.21x10^{4}$	0.860
50	$8.38x10^{-1}$	$1.60x10^{15}$	$2.44x10^{-1}$	1.11	$8.27x10^{-5}$	$2.21x10^{4}$	0.863
70	$8.60x10^{-1}$	$1.61x10^{15}$	$2.44x10^{-1}$	1.13	$8.34x10^{-5}$	$2.25x10^{4}$	0.885
100	$8.62x10^{-1}$	$1.61x10^{15}$	$2.44x10^{-1}$	1.13	$8.37x10^{-5}$	$2.24x10^{4}$	0.887
200	$8.72x10^{-1}$	$1.60x10^{15}$	$2.44x10^{-1}$	1.14	$8.44x10^{-5}$	$2.25x10^{4}$	0.897
300	$8.96x10^{-1}$	$1.60x10^{15}$	$2.44x10^{-1}$	1.17	$8.55x10^{-5}$	$2.28x10^{4}$	0.921
400	$9.05x10^{-1}$	$1.60x10^{15}$	$2.44x10^{-1}$	1.17	$8.61x10^{-5}$	$2.29x10^{4}$	0.930
500	$9.12x10^{-1}$	$1.59x10^{15}$	$2.44x10^{-1}$	1.18	$8.66x10^{-5}$	$2.30x10^{4}$	0.937
700	$9.34x10^{-1}$	$1.58x10^{15}$	$2.45x10^{-1}$	1.20	$8.79x10^{-5}$	$2.32x10^{4}$	0.959
1000	$9.97x10^{-1}$	$1.59x10^{15}$	$2.44x10^{-1}$	1.27	$9.06x10^{-5}$	$2.40x10^{4}$	1.020

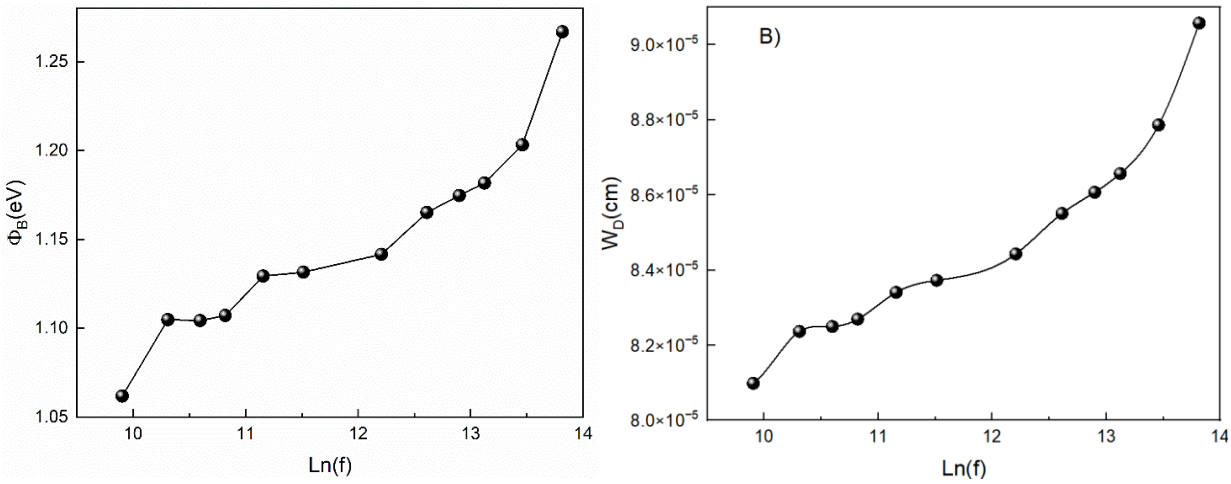


Figure 7. Variation of the Φ_B, and W_D as a function of frequency.

The results presented in Table (1) and Fig. 7 show that the extracted electrical parameters exhibit different degrees of frequency dependence. As the extracted Φ_B, N_D, V_D, and E_m generally increase. In contrast, the donor concentration remains nearly constant, while the Fermi-level position changes only slightly over the investigated frequency range.

The observed frequency dependence may be related to the response of interface states, interfacial polarization, and the relaxation process within the structure. At low frequencies, dipolar polarization and electrically active interface states can respond more effectively to to the AC signal, conturbuting to the measured electrical response. Under these conditions, interface states can actively exchange charge with the semiconductor and contribute to the measured capacitance, thereby affecting the extraction of the electrical parameters. As the frequency increases, some interface states and polarization processes can no longer follow the applied AC signal, reducing their contribution to measured capacitance. Consequently, the measured capacitance becomes less sensitive to slowly responding interface states and polarization process, while the depletion-layer contribution becomes more prominent. The frequency-dependence variation in the extracted electrical parameters should therefore be interpreted with caution, since the measured capacitance may be influenced by interface states, the interface layer, and series resistance. The increase in extracted barrier height and related parameters may be associated with the response of interface states and other non-ideal effects, rather than necessarily reftecting a change in the intrinsic properties of the metal–semiconductor junction.

The capacitance and extracted parameters depend on both frequency and bias voltage. This behavior may reflect the combined effect of interface states, dielectric relaxation, *Rs*, polarization, and the interfacial layer. The frequency dispersion in the depletion and inversion regions may be associated with interface states and polarization effects, particularly at low and intermediate frequencies. At higher frequencies, series resistance may have a strong influence on the measured response in the accumulation region. The capacitance and extracted electrical parameters depend on both frequency and bias voltage. This behavior may reflect the combined effects of interface states, dielectric relaxation, series resistance, polarization, and the interfacial layer. The frequency dispersion in the depletion and inversion regions may be associated with interface state and polarization effects, particularly at low and intermediate frequencies. At higher frequencies, series resistance may have a stronger measured response in the accumulation region.

The results demonstrated that interface-related effects and series resistance contribute to the voltage- and frequency-dependent electrical response of fabricated structure. The frequency dispersion observed in the capacitance and conductance characteristics is consist with a contribution from electrically active interface states and their interaction with charge carriers. Such interfacial activity influences the electrical response of the device to external perturbations and may be relevant to sensing application. In particular, the interface-dominated behavior observed in Al/CuO/p-Si structure may provide useful insights into its potential use in CuO-based sensor applications, where interfacial properties can influence the electric response. The interface-state density was estimated using the C_{LF}-C_{HF} model, Hill-Coleman method, and parallel conductance technique. The differences between the extracted values highlight the importance of considering the assumptions and limitations of each method. The observed low-frequency capacitance response indicates the importance of interface-related effects in the electrical behavior of the structure. The results indicate that frequency-dependent electrical behavior should be considered when evaluating Al/CuO/n-Si Schottky structures, particularly because of the influence of interface effects.

The voltage and frequency dependence of the series resistance, (Rs), was investigated using the Nicollian& Brews approach, which is given in Figure 8. The method is described by the following equation [2,36]:

$$R_s = \frac{G_m}{[{G_m}^2 + ({G_m}^2 + (\omega C_m)^2)]} \quad (5)$$

Here *Gm* and *Cm* are the measured conductance and capacitance values at given bias voltage, respectively, and ω (=2πf) is the angular frequency.

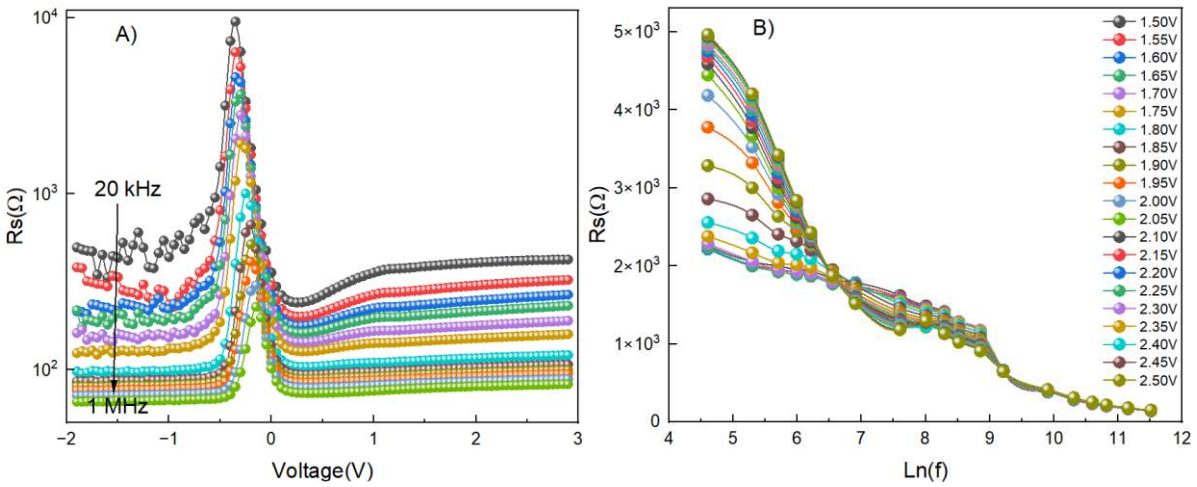


Figure 8. (a) R_s vs. V and (b) R_s vs. Ln(f) plots of the Al/CuO/n-Si *SBD*.

The *Rs-V* characteristics show a dependence on measurement frequency, and a resistance peak is observed near 0 *V*. The peak may be attributed to the combined effects of interface states, and charge redistribution at the interface. However, the present data do not allow the contribution of each mechanism to be determined separately. The peak becomes less pronounced as the frequency increases. This trend is consistent with a reduced contribution from interface states at higher frequencies, although other frequency-dependent effects may also influence the measured resistance. The results suggest that the influence of *Rs* varies with bias voltage and becomes more apparent in the accumulation region. Its contribution should be considered when interpreting the measured capacitance and conductance, particularly at higher frequencies. To determine the effects of *Rs* on the measured admittance, the *C-V* and *G-V* characteristics at 1 *MHz* were corrected using Nicollian and Brews approach, as expressed below [2,36]:

$$C_c(V) = \frac{[{G_m}^2 + (\omega C_m)^2]C_m}{a^2 + (\omega C_m)^2} \quad (6a)$$

$$G_c(V) = \frac{[G_m{}^2+(\omega C_m)^2]a}{a^2+(\omega C_m)^2} \quad (6b)$$

Here a is the correction factor that varies as a function of the Rs, and can be expressed as follows:

$$a = G_m - [G_m{}^2 + (\omega C_m)^2]R_s \quad (6c)$$

Using Eqs. (6a–c), the measured C_m and G_m/ω data were corrected over the investigated voltage range. The corrected characteristics are presented in Fig. 9. After correction, the corrected capacitance (*Cc*) increases with applied bias voltage in the depletion and weak accumulation regions, in contrast to the trend observed in the measured capacitance. The corrected conductance, *Gc/ω,* also displays a distinct peak in the depletion region. The differences between the measured admittance and corrected curves indicate that the *Rs* affects the measured admittance, particularly in the accumulation region at 1 MHz.

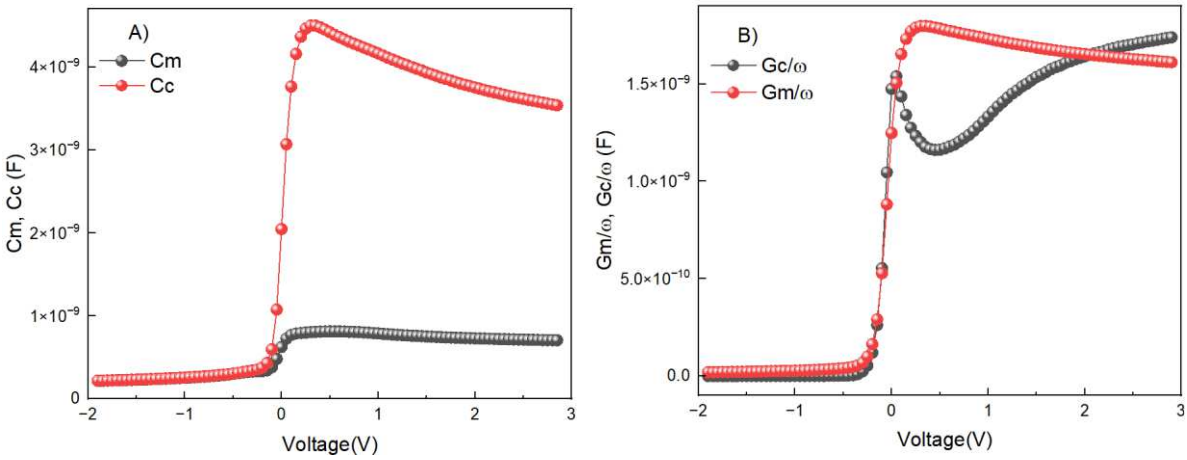


Figure 9. Comparison between measured (C_m, G_m) and corrected (C_c, *Gc*) of the Al/CuO/n-Si *SBD*.

Several models can be used to estimate the interface-state density (*Nit*), from bias voltage- and frequency-dependent *C-V* and *G-V* measurements. In this study, *Nit* was estimated using the high-low frequency capacitance method (C_{HF}-C_{LF}) [36], the Hill-Coleman method [37], and the parallel capacitance model [2,36]. These methods rely on different aspects of measured electrical response and may therefore yield different estimates but the conditions for applying these models differ slightly.

The C_{HF}-C_{LF} method uses capacitance values measured at low and high frequencies. In this study, the low- and high-frequency values were taken at 1 kHz and 1 MHz, respectively. The method assumes that the contricution of interface states differs between these two measurement conditions. The Hill–Coleman model was used to estimate *Nit* from the measured capacitance and conductance data. The C_{LF}–C_{HF} model, which is based on (C_{LF} = 1 *kHz*) and C_{HF} =1 *MHz*), was used to derive the voltage-dependent Nit based on the following relations [36]:

$$N_{it}(V) = \frac{1}{(qA)}.\left[\left(\frac{1}{C_{LF}} - \frac{1}{C_i}\right)^{-1} - \left(\frac{1}{C_{HF}} - \frac{1}{C_i}\right)^{-1}\right] \quad (7)$$

The interlayer-capacitance (C_i) was estimated from measured high-frequency capacitance (C_m) and conductance (G_m) using the relation given below [17]:

$$C_i = C_m\left(1 + \frac{G_m^2}{\omega^2 C_m^2}\right) = \frac{\varepsilon_i \varepsilon_o A}{d_i} \quad (8)$$

The extracted Nit varies with applied voltage, indicating that the measured contribution of interface state depends on the electrical bias. As Figure 10 shows, the extracted Nit increases with applied voltage and reaches a maximum value of approximately 3.3×10^{10} $eV^{-1}cm^{-2}$ near 1.7 V, before decreasing at higher voltages. This peak may be related to the difference between the low- and high-frequencies responses, which is used to estimate the contribution of interface states in the C_{LF}–C_{HF} model. At high voltages, the extracted Nit decreases, suggesting a lower contribution from interface states to the measured capacitance response under these conditions. The observed variation indicates that the electrical contribution of interface states changes with the applied bias, although their energy distribution across the semiconductor bandgap and cannot be determined from this curve alone.

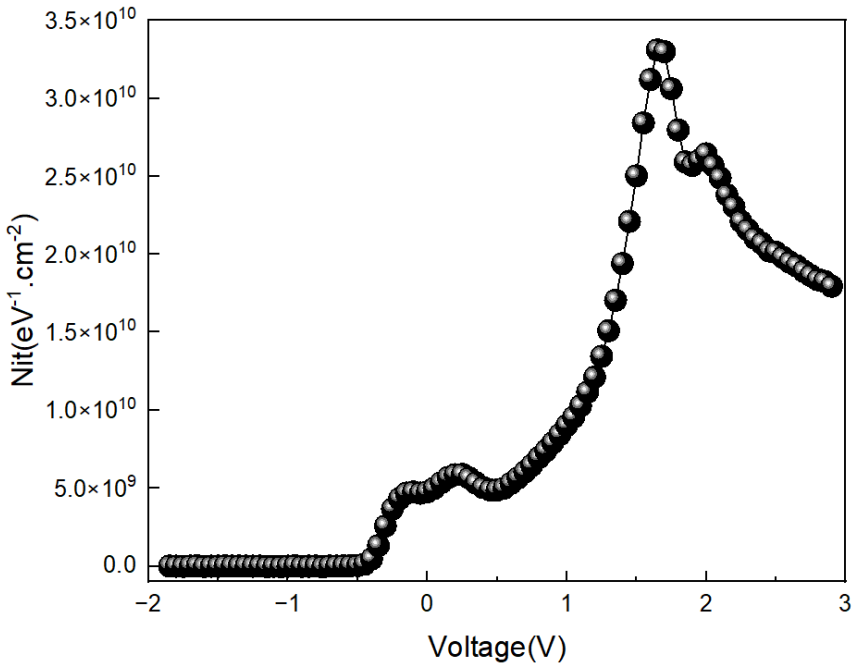


Figure 10. The *Nit-V* plot of the Al/CuO/n-Si *SBD* was extracted from the C_{HF}-C_{LF} model.

The interface-state density was also estimated using the Hill-Coleman method [37], which relates Nit to the measured capacitance and conductance as expressed in the following equation:

$$N_{it} = \left(\frac{2}{qA}\right)\frac{(G/\omega)_{max}}{[(G/\omega)_{max}/C_i]^2+(1-C_{max}/C_i)^2} \quad (9)$$

In Eq.(9), (A) is the Schottky contact area, while G_{max}/ω is the maximum measured conductance divided by the angular frequency, C_{max} is the capacitance measured at the corresponding bias voltage, and *Ci* is the interlayer capacitance estimated using Eq. (8). The *Nit* values calculated using Eq.(9) are summarized in Table 2.

Table 2. Interface state density (N_{it}) values calculated using the Hill-Coleman method at different frequencies.

Frequency (Hz)	Ln (f)	V_m (V)	G_{max}/ω (nF)	C_{max} (nF)	N_{it} ($\times10^{13}$) ($eV^{-1}.cm^{-2}$)
200	5.29	1.70	99.3	137.0	8.14
300	5.70	2.00	78.0	138.0	6.98
400	5.99	2.05	71.5	106.0	6.13

500	6.21	2.10	65.7	89.6	5.34
700	6.55	2.30	60.4	67.1	4.18
1000	6.90	2.35	51.0	55.7	3.28
2000	7.60	2.45	35.2	44.0	2.29

As shown in Fig.11 (a,b), the *Nit* values extracted using the Hill-Coleman method decrease with increasing frequency. This trend is consistent with a reduced contribution from interface states that cannot follow the faster AC signal. At low frequencies, interface states with suitable time constants can exchange charge with the semiconductor during the Ac cycle. As the frequency increases, some of these states can no longer respond fully to the applied signal. The extracted *Nit* also decreases with increasing bias voltage over the measured range, indicating that the contribution of interface states to the measured response charges with the electrical bias. Furthermore, the stronger electric field at higher voltages improves the separation of charge carriers and reduces the effect of some trap centers on the capacitance response, which is reflected in a decrease in the density of interstates.

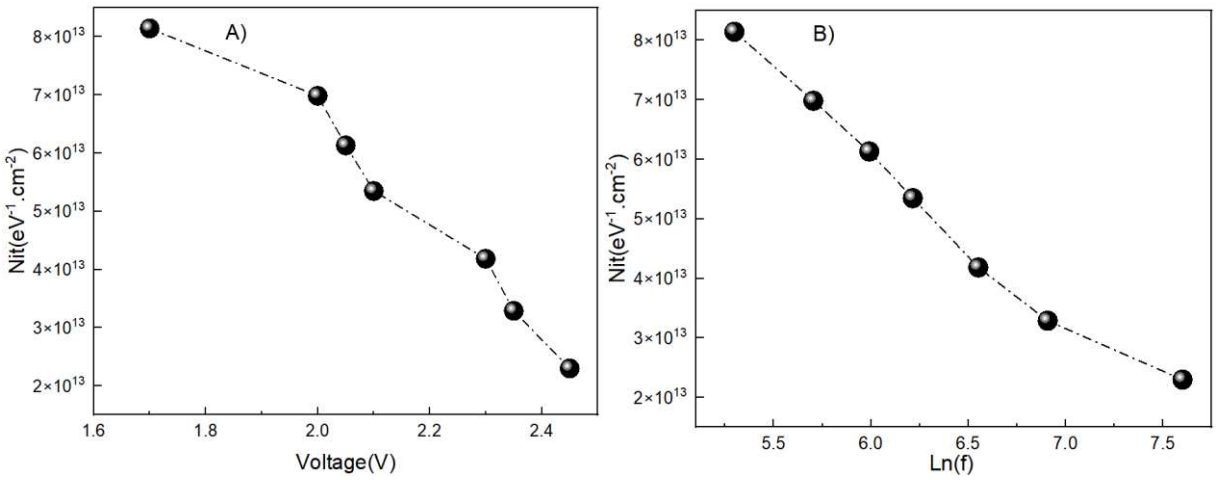


Fig 11. Variation of extracted interface-state density (Nit) as a function of a) applied voltage, and Ln(f), determined using the Hill-Coleman method.

To examine the frequency dependence of electrical response, the measured C and Gm/ω values were plotted against *ln f* at bias voltages ranging from 0.2 to 1.6 V, as shown in Fig. 12. The measured capacitance decreases with increasing frequency at the investigated bias voltages.

This behavior may be related to the reduced response of interface states and polarization processes to faster AC signal at high frequencies.

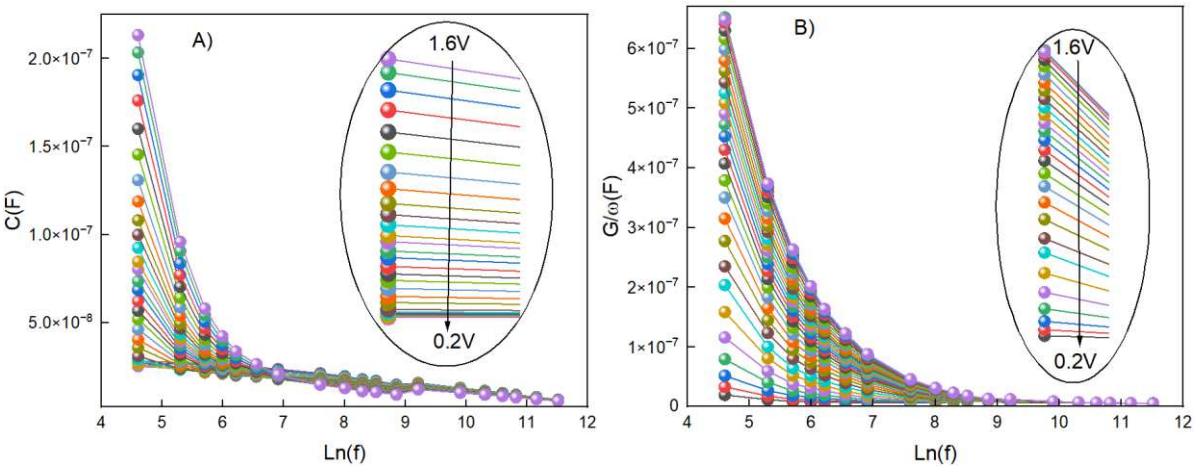


Figure 12. Frequency dependence of **(a)** the measured capacitance (*C)* and **(b)** the conductance divided by angular frequency (*Gm/ω*) against Ln(f) at bias voltages ranging from 0.2 to 1.6 V.

The parallel conductance method was used to obtains *Nit* and the relaxation time constant (τ) as a function of bias voltage. For this purpose, the *Gp/ω* versus *ln f* curves were calculated from the measured capacitance and conductance data using Eqs. (10a) and (10b), as shown in Fig. 13. The *Gp/ω-ln f* curves exhibit distinct peaks at different frequencies for the applied bias voltages. The peak frequency can be used to estimate the interface-state relaxation time (ωτ= 1.98) from the peak condition specified by the parallel conductance model [3,17].

These peaks reflect the charge-exchange processes between the interface traps and the conduction or valence band in the semiconductor, and the shift of their positions with the bias voltage indicates that both the *Nit* and their τ depend on the applied electric field and the position of the Fermi level at the interface.

$$\frac{G_p}{\omega} = \frac{\omega C_i^2 (G_m - \omega^2 C_m^2 R_s - R_s G_m^2)}{(\omega^2 C_i R_s C_m - G_m)^2 + \omega^2 (C_i - C_m - C_i R_s G_m)^2} = \frac{qAN_{it}}{2\omega\tau} \ln(1 + (\omega\tau)^2) \qquad (10a)$$

$$N_{it} = \left(G_p/\omega\right)_{max} / (0.402qA) \qquad (10b)$$

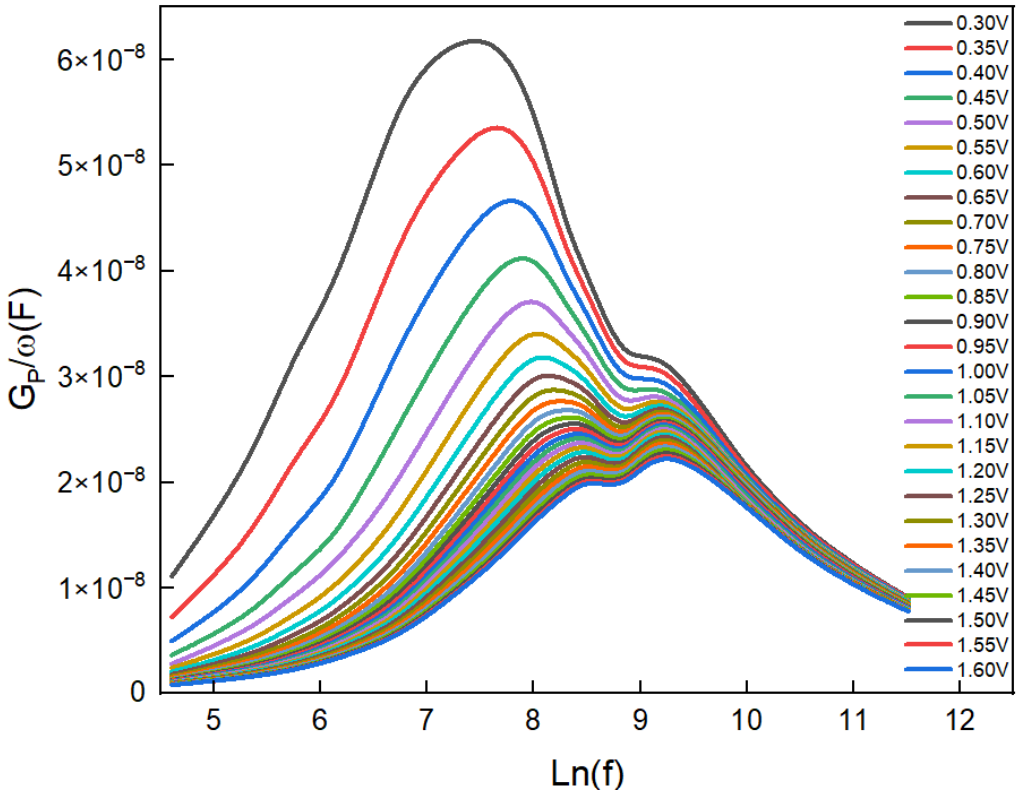


Figure 13. The G_p/ω versus Ln(f) curves of the Al/CuO/n-Si Schottky structure at different bias voltages.

As the applied voltage increases, the extracted *Nit* and τ decrease over the investigated bias range. The pronounced decrease at the low bias voltage suggest that the electrical response of interface states charges as the bias condition at the CuO/Si interface are modified. Simultaneously, a reduced τ indicates faster carrier trapping and emission, pointing to enhanced charge exchange at the semiconductor-interface boundary. At higher voltages, the charges in both parameters become less pronounced, suggesting a weaker variation in the extracted interface-states response over this part of the bias range. The simultaneous reduction in *Nit* and τ demonstrates that the extracted interface-state parameters vary with forward bias, and these trends show that charge transport improves and trap-assisted recombination reduces under higher forward bias conditions.

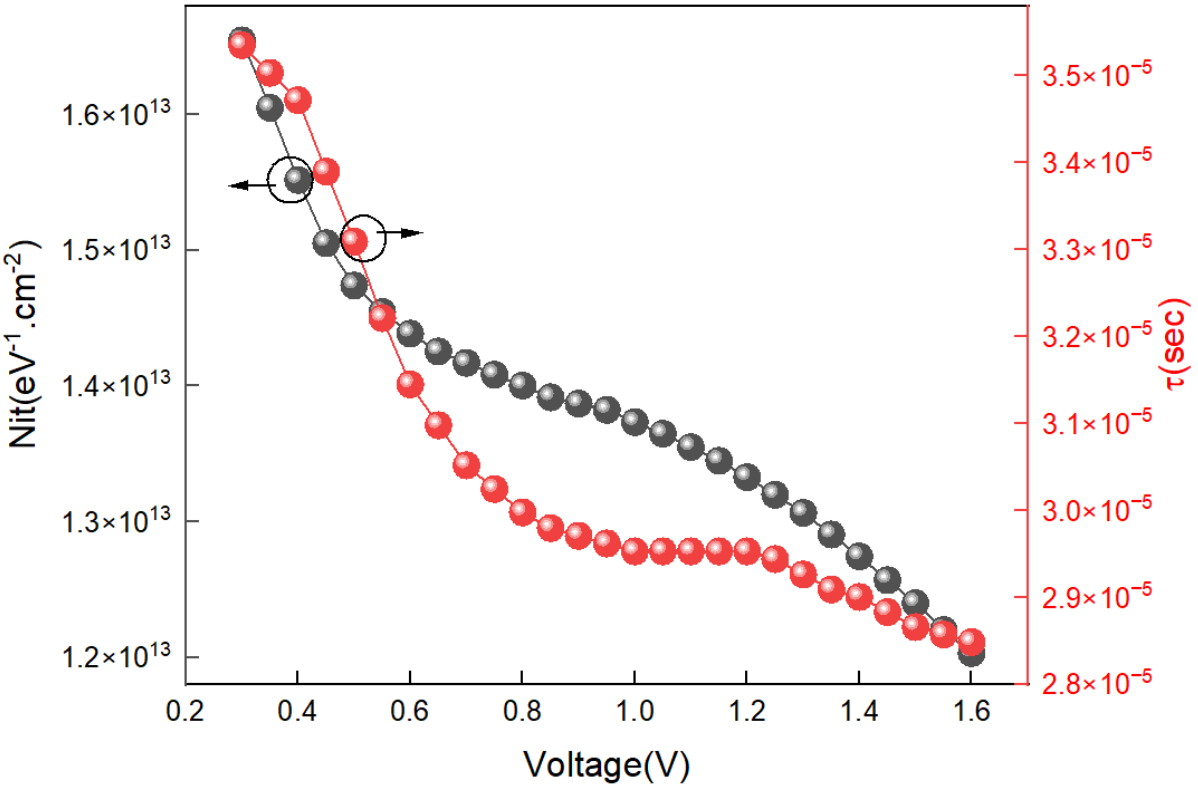


Figure 14. Bias-voltage dependence of the interface-state density (N_{it}) and relaxation time constant (τ) extracted using the parallel conductance method.

The three methods yield different *Nit* values and voltage-dependent trends, both in magnitude and in curve shape. These differences may arise from the district assumption of each method and their different sensitivities to the frequency-dependent response of interface states distribution of interfacial trap states within the semiconductor bandgap and the τ associated charge capture/ release processes. The C_{LF}–C_{HF} method relies on capacitance values measured at low frequencies, whereas the Hill-Coleman and parallel conductance methods also use conductance-related information to estimate interface-state response. The observed variations among the extracted results have been widely reported and critically examined in recent literature [15,36,38-40]. Such discrepancies are generally attributed to the intrinsic assumptions and limitations associated with each analytical approach, together with the fact that different methods probe different energy distributions of interface states within the semiconductor bandgap and exhibit varying sensitivities to their dynamic response characteristics.

Conclusion

This study examines the voltage- and frequency-dependent electrical characteristics of Al/CuO/n-Si Schottky structure using *C-V* and *G-V* measurements over a broad frequency range. The results show that the measured electrical response of the fabricated devices is strongly influenced by interface state density, surface charge effects, and series resistance, with their contributions varying with bias voltage and frequency. The frequency dispersion observed in both capacitance and conductance characteristics is consistent with a contribution from electrically active interface states and their response to the applied AC signal. The interface state density was evaluated using the C_{LF}–C_{HF} model, Hill–Coleman method, and parallel conductance method, allowing the results obtained from different approaches to be compared. The differences between the obtained values highlight need to consider assumptions and limitations of each method when interpreting interface-state density. Furthermore, the observed interface-related effects may be relevant the potential for charge-sensitive and surface-controlled device applications. These results provide valuable insight into the importance of accounting for frequency-dependent effects and series resistance when interpreting the electrical characteristic of Al/CuO/n-Si Schottky structures.

Data availability: All data generated or analyzed during this study are included in this published article. Additional data or materials related to this work are available from the corresponding author upon reasonable request.

Author Contributions: İ.C. wrote and edited the manuscript, contributed to the interpretation of the results, and supervised the study. F.M.C. performed the experimental work and prepared the devices. A.A.E. contributed to the experimental work, assisted in device preparation, and contributed to the preparation of the manuscript. S.A.H. performed the electrical measurements and corresponding calculations and analyses, and contributed to drafting the manuscript. S.E.S. reviewed the final version of the manuscript and contributed to the supervision of the study. Ş.A. supervised the study and critically reviewed the manuscript.

Funding Declaration: This work is partially supported by the research project FKA-2024-3939 of Kocaeli University.

Declarations: İdris CANDAN, Fatih Mehmet Coşkun, Sabreen A. Hameed, Abeer AL-Edresi, Sait Eren San, and Şemsettin Altındal stated that they have no known competing financial interests or personal relationships that could be perceived as influencing the work reported in this paper.

References

[1] S.M. Sze, K.K. Ng, Physics of Semiconductor Devices, 3rd ed. (Wiley, New York, 2007).

[2] E.H. Nicollian and J.R. Brews, MOS (Metal Oxide Semiconductor) Physics and Technology (Wiley, New York, 1982).

[3] T.K.S. Wong, S. Zhuk, S. Masudy-Panah, and G.K. Dalapati, Materials 9, 271 (2016).

[4] S.M. Abzal, J.K. Dash, C. Mahata, A. Guchhait, A. Kumar, S. Ramakrishna, and G.K. Dalapati, J. Electron. Mater. 50, 1720 (2021).

[5] S. Masudy-Panah, G.K. Dalapati, K. Radhakrishnan, A. Kumar, and H.R. Tan, J. Appl. Phys. 116, 074501 (2014).

[6] A. Tombak, M. Benhaliliba, Y.S. Ocak, T. Kılıçoğlu, Results Phys. 5, 314 (2015).

[7] J. Sultana, A. Das, A. Das, N.R. Saha, A. Karmakar, S. Chattopadhyay, Thin Solid Films 612, 331 (2016).

[8] A. Badawi, S.S. Alharthi, M.G. Althobaiti, A.N. Alharbi, H. Assaedi, H.I. Alkhammash, N. Al-Hosiny, Appl. Phys. A 127, 235 (2021).

[9] E.H. Rhoderick, R.H. Williams, Metal-Semiconductor Contacts, 2nd ed. (Oxford University Press, Oxford, UK, 1988).

[10] T.V. Pham, M. Rao, P. Andreasson, Y. Peng, J. Wang, K. Jinesh, Appl. Phys. Lett. 102, 032101 (2013).

[11] M. Heinemann, B. Eifert, C. Heiliger, Phys. Rev. B 87, 115111 (2013).

[12] S.C. Ray, Sol. Energy Mater. Sol. Cells 68, 307 (2001).

[13] M. Kevin, W.L. Ong, G.H. Lee, G.W. Ho, Nanotechnology 22, 235701 (2011).

[14] M.F. Al-Kuhaili, Vacuum 82, 623 (2008).

[15] A. Abidinov, I. Afandiyeva, E. Bakhtiyarli, S. Altındal Yerişkin, S.A. Hameed, ACS Appl. Electron. Mater.7, 9399 (2025).

[16] V. Figueiredo, E. Elangovan, G. Gonçalves, P. Barquinha, L. Pereira, N. Franco, E. Alves, R. Martins, E. Fortunato, Appl. Surf. Sci. 254, 3949 (2008).

[17] H.S. Kim, J.W. Lim, S.J. Yun, M.A. Park, S.Y. Park, S.E. Lee, H.C. Lee, Jpn. J. Appl. Phys. 52, 10MB17 (2013).

[18] S. Mridha, D. Basak, Semicond. Sci. Technol. 21, 928 (2006).

[19] T. Ishihara, M. Higuchi, T. Takagi, M. Ito, H. Nishiguchi, Y. Takita, J. Mater. Chem. 8, 2037 (1998).

[20] S. Baturay, I. Candan, C. Özaydın, Research Square (2021).

[21] S. Karthick Kumar, S. Suresh, S. Murugesan, S.P. Raj, Sol. Energy 93, 221 (2013).

[22] K. Neyvasagam, R. Chandramohan, S. Valanarasu, A.M.F. Benial, J. Mater. Sci.: Mater. Electron. 26, 8489 (2015).

[23] Y.S. Chaudhary, S.A. Khan, C. Tripathi, R. Shrivastav, V.R. Satsangi, S. Dass, Nucl. Instrum. Methods Phys. Res. Sect. B 330, 1 (2014).

[24] L.C. Chen, C.C. Chen, K.-C. Liang, S.-H. Chang, Z.L. Tseng, S.C. Yeh, C.T. Chen, W.T. Wu, C.G. Wu, Nanoscale Res. Lett. 11, 402 (2016).

[25] İ. Candan, M. Parlak, Ç. Erçelebi, J. Mater. Sci.: Mater. Electron. 30, 2127 (2019).

[26] M. Abdelfatah, J. Ledig, A. El-Shaer, A. Wagner, V. Marin-Borras, A. Sharafeev, P. Lemmens, M.M. Mosaad, A. Waag, A. Bakin, Sol. Energy Mater. Sol. Cells 153, 157 (2016).

[27] Ö. Bayraklı Sürücü, H.H. Güllü, M. Terlemezoglu, D.E. Yildiz, M. Parlak, Physica B 570, 246 (2019).

[28] M. Abdelfatah, J. Ledig, A. El-Shaer, A. Sharafeev, P. Lemmens, M.M. Mosaad, A. Waag, A. Bakin, ECS J. Solid State Sci. Technol. 5, Q183 (2016).

[29] B. Akın, S.A. Hameed, S.A. Yerişkin, M. Ulusoy, H. Durmuş, Mater. Sci. Semicond. Process. 184, 108781 (2024).

[30] M. Abdelfatah, A. El-Shaer, Mater. Lett. 210, 366 (2018).

[31] A. El-Shaer, M. Abdelfatah, K.R. Mahmoud, S. Momay, M.R. Eraky, J. Alloys Compd. 817, 152799 (2020).

[32] I.M. Afandiyeva, E.R. Bakhtiyarli, S. Altındal Yerişkin, S.A. Hameed, Thin Solid Films 839, 140916 (2026).

[33] K. Yıldız, S. Altındal Yerişkin, S.A. Hameed, E. Erbilen Tanrıkulu, F. Yakuphanoğlu, J. Mater. Sci.: Mater. Electron. 36, 2204 (2025).

[34] A. Tombak, M. Benhaliliba, Y.S. Ocak, T. Kılıçoğlu, Results Phys. 5, 314 (2015).

[35] K.A. Jagadish, D. Kekuda, Mater. Res. Express 12, 096404 (2025).

[36] Ç. Güçlü, S.A. Hameed, A. Khalkhali, İ. Taşçıoğlu, Ş. Altındal, J. Mater. Sci.: Mater. Electron. 36, 853 (2025).

[37] W.A. Hill, C.C. Coleman, Solid-State Electron. 23, 987 (1980).

[38] A. Roy, Discov. Electron. 3, 4 (2026).

[39] E.H. Nicollian, A. Goetzberger, Bell Syst. Tech. J. 46, 1055 (1967).

[40] S.A. Hameed, Ö. Berkün, S.A. Yerişkin, Gazi Univ. J. Sci. Part A Eng. Innov. 11, 235 (2024).